DOI: 10.1002/ejic.201000070

Flower-Like Nickel Nanocrystals: Facile Synthesis, Shape Evolution, and Their Magnetic Properties

Pengwei Li,[a] Ning Wang,*[b] and Rongming Wang*[a]

Keywords: Nickel / Nanostructures / Solution synthesis / Magnetic properties

In this paper, flower-, star-, and chain-like hierarchically nanostructured nickel crystals as well as $[Ni(N_2H_4)_2]Cl_2$ nanorods were first synthesized by a simple reduction method. This method is template-free, environmentally benign, and can be carried out at low temperature (60 °C) with high efficiency on a large scale. Investigation of the growth kinetics has proved that the crystal sizes are sensitive to the reaction temperature and reaction time. Various nickel nanostructures can be achieved by the oriented growth of preferred nickel crystal planes. The magnetic properties of the flower-like nickel nanocrystals were also characterized with the results of much enhanced coercivity (Hc) and decreased saturation magnetization (Ms).

Introduction

Currently, three-dimensional (3D) nanomaterials of metals and metal oxides that are derived from low-dimensional nanowires, nanorods, and nanotubes have attracted increasing attention due to shape-dependent chemicophysical properties. In comparison to their low-dimensional counterparts, the hierarchical nanostructures exhibit not only high surface-to-volume ratios, but also excellent structural stabilities and spatial uniformity, which makes them strong candidates for wide applications in photonics, nanoelectronics, catalysts, biosensors, and so on.[1–6]

As an important functional material, Ni is promising in catalysis, magnetic sensors, high-density magnetic records and many other domains.[7–10] Motivated by the belief that the physical and chemical properties of these nanoparticles depend strongly on their size and shape, considerable efforts have been devoted to prepare nickel nanocrystals with special morphologies.[11–15] Various strategies, such as solution reduction, electrodeposition, as well as magnetic-field induction, have been extensively explored for the precisely controlled construction of novel nickel nanostructures.[16–19] Among all the methodologies, the wet chemical route has been proved to be especially effective and facile for the synthesis of nickel nanocrystals. However, in contrast with the extensive work on the synthesis of low-dimensional nickel nanocrystals, reports on the template-free multidimensional construction of nickel nanostructures are rather rare,[20] and little work has been focused on the growth mechanism of hierarchical nickel nanostructures in the absence of hard templates or surfactants.

Herein, we report a facile synthesis of hierarchically nanostructured nickel crystals with high yield. The novelty of this work is characterized by a one-pot procedure that combines sequential formation of precursor chelation, nucleation, and morphology shaping under mild solution conditions without any surfactants, hard templates, or external fields. In addition, the magnetic properties of these flower-like nanostructures are also reported.

Results and Discussions

The powder XRD pattern of the as-prepared product is shown in Figure 1. All the diffraction peaks can be indexed as pure-phase metallic Ni with a face-centered cubic (fcc) structure (JCPDF No. 04-0850, a = 0.3521 nm). It is worth noting that the intensities between the (200) and (111) diffraction peaks is somewhat lower than the conventional value (0.32 to 0.42), which indicates that our products may

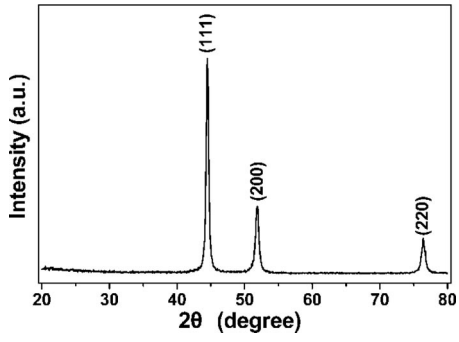

Figure 1. The XRD patterns of the as prepared Ni products.

[a] Key Laboratory of Micro-nano Measurement, Manipulation and Physics (Ministry of Education) and Department of Physics, Beijing University of Aeronautics and Astronautics, Beijing 100191, People's Republic of China
E-mail: rmwang@buaa.edu.cn
[b] School of Chemistry and Environmental Engineering, Beijing University of Aeronautics and Astronautics, Beijing 100191, People's Republic of China
E-mail: wangning@buaa.edu.cn

be abundant in {111} facets, and the nickel nanocrystals may grow with preferred orientation along the (111) direction.

As can be seen from Figure 2a,b, nickel crystals of a flower-like hierarchical structure with a petal length of about 300–500 nm have been successfully synthesized on a large scale and with high uniformity. Figure 2c reveals that the base width is about 50 nm with a tip size of no more than 10 nm.

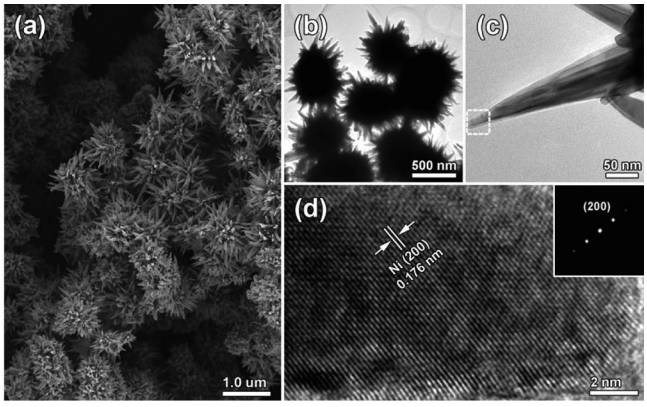

Figure 2. Typical SEM and TEM images of the as-obtained Ni nanoflowers: (a, b) Overhead view, (c) magnified view of acicular branch, (d) HRTEM image at the tip of the acicular branch and the inset corresponding FFT pattern for the HRTEM image.

Figure 2d is the HRTEM image of the framed area in Figure 2c. The parallel lattice fringes go through the tip of the petal, and the distance is measured to be about 0.176 nm, which matches well with the d_{200} value of fcc Ni. The Fast Fourier Transform (FFT) pattern arranged in the inset of Figure 2d shows the crystalline features of the sample. The dominant growth of the {200} planes of the petal indicates that the crystal growth along the crystal face with lower surface energy (200 vs. 222) is preferred at such a low temperature (60 °C) as expected from the XRD pattern.

Superstructures that spontaneously form might provide materials with new properties. The investigations on the properties and growth should be interesting and relevant. Figure 3a reveals the rod-like morphology of the intermediate products (obtained at a reaction time of 10 min), which have lengths varying from 300 to 500 nm and diameters of about 50 nm. Figure 3b shows that star-like Ni nanostructures began to appear in about 20 min, which were then crystallized to Ni nanostars (at a reaction time of 1 h) with a pod length of about 300–500 nm. Finally, all rod-like intermediates transform into flower-like Ni nanocrystals (40 min), as shown by Figure 3c. All diffraction peaks (marked with a diamond) for the intermediate products within Figure 3d can be indexed to $[Ni(N_2H_4)_2]Cl_2$ (JCPDF card no. 28-0695), whereas patterns marked with "b" are associated with typical fcc Ni (JCPDF card no. 04-0850). Thus, the stepwise evolution from the intermediate $[Ni(N_2H_4)_2]Cl_2$ nanorods into Ni nanoflowers was observed. The chemical reactions for the formation of the flower-like Ni nanostructures in a nonalkaline system can be expressed by Equations (1) and (2).

$$Ni^{2+} + 2N_2H_4 \rightarrow [Ni(N_2H_4)_2]^{2+} \quad (1)$$

$$2[Ni(N_2H_4)_2]^{2+} + 4N_2H_4 \rightarrow 2Ni\downarrow + 3N_2\uparrow + 10NH_3\uparrow + 2H^+ \quad (2)$$

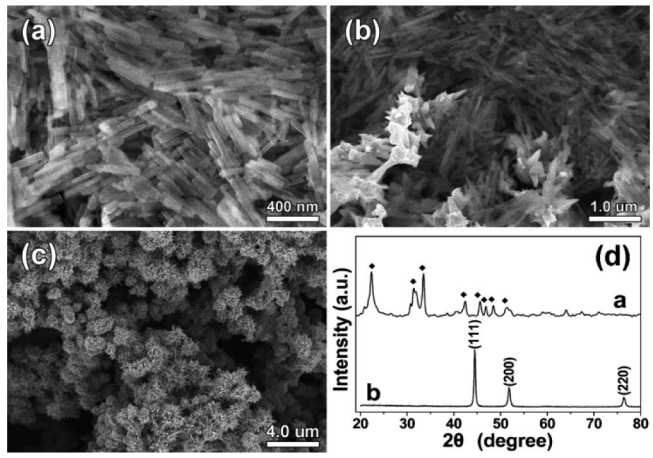

Figure 3. SEM images of the products with reaction times of (a) 10 min, (b) 20 min, and (c) 40 min. (d) Comparisons between the XRD patterns for the intermediate rod-like and flower-like products.

Results of temperature dependence experiments are shown in Figure 4, and the products obtained at elevated temperatures have morphologies far different from that of the initial one. First, products obtained at higher temperature were small particles, which further self-assembled into chain- or nestle-like aggregates (Figure 1a). Second, the sizes of the particles change from 80, 40, and 50 to 60 nm, and the size of the side branch decreased from about 100–200 nm to 20 nm when the temperature was increased from 120 to 200 °C. Here, the size of the nickel crystals shows a positive correlation with the reaction temperature at elevated temperature (120 to 200 °C), whereas a negative correlation is seen in the temperature range below 80 °C. This

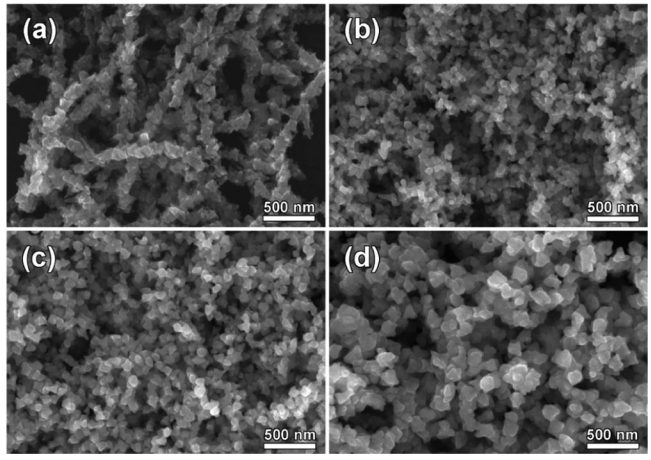

Figure 4. Typical SEM images of the chain-like products synthesized at different reaction temperatures: (a) 80 °C, (b) 120 °C, (c) 160 °C, and (d) 200 °C.

phenomenon is interesting, which should be interpreted by surface energies associated with the fcc crystal. Surface energies associated with the fcc crystal are usually different and can be elucidated in a general sequence as {111} > {100} > {110}. The shape of such a fcc nanocrystal is mainly determined by the ratio (R) of the growth rate along (100) to the (111) direction. In our case, at elevated temperature, the shape transformation from flower to multipod star should be a sign that growth of the {100} planes was thermodynamically restrained, and growth of the {111} plane with higher surface energy became dominant. In other words, higher reaction temperatures make the growth of crystal planes with higher surface energies favorable.

Concentration-dependent parallel experiments were also conducted (0.005, 0.01, 0.1, and 0.5 M). At low temperatures such as 60 °C, the morphologies of the products do not undergo any obvious change with different concentrations. When the temperature increases, the size of the nickel crystals has distinctive differences. Figure 5 shows the typical SEM morphologies of the samples obtained at 160 °C. The nickel chains with starfish-like building blocks remained almost unchanged, whereas the size of the particles grows significantly from 40 nm to about 300 nm with increased salt concentrations. A higher concentration of the precursor results in larger nickel nanoparticles (Figure 5b–d). From a standpoint of the growth kinetics, with higher concentration, both the formation of small nuclei and their transformation into larger crystals are kinetically and thermodynamically favored.

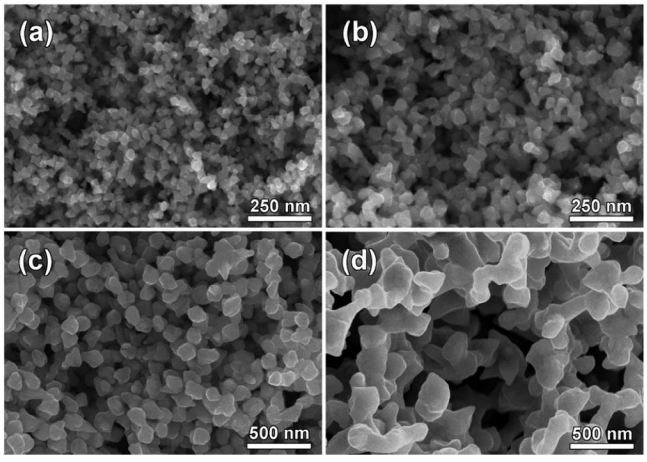

Figure 5. SEM images of the products obtained at different concentrations: (a) 0.005, (b) 0.01, (c) 0.1, and (d) 0.5 M.

Typical TEM and SEM characterizations (200 °C, concentration of the metal precursor remained as 0.1 M) of the nickel nanostructures are further made to show the temperature-dependent effect on crystal morphologies (Figure 6). The as-prepared nickel nanocrystals are of chain- or nestle-like shape with a center size of about 30 nm and side-branch lengths of 10 to 20 nm. TEM images (Figure 6a,b) verify the starfish-like morphology of the nickel nanocrystals. It can be seen that the nickel nanocrystals grow in several directions to form rod-like branches with lengths of ca. 20 nm. The interplanar spacings are measured to be 0.203 nm, which fits well with the d value between the {111} planes of fcc Ni crystal. Coherent and small angle grain boundaries between the nanocrystallines can be found in the HRTEM image, whereas the SAED pattern (Figure 6c) shows a polycrystalline nature of the pure metallic fcc Ni nanoparticles. This observation suggests the formation of larger nanoparticles with greater volume but lower energy state, at the expense of the depletion of small particles as nutrients.

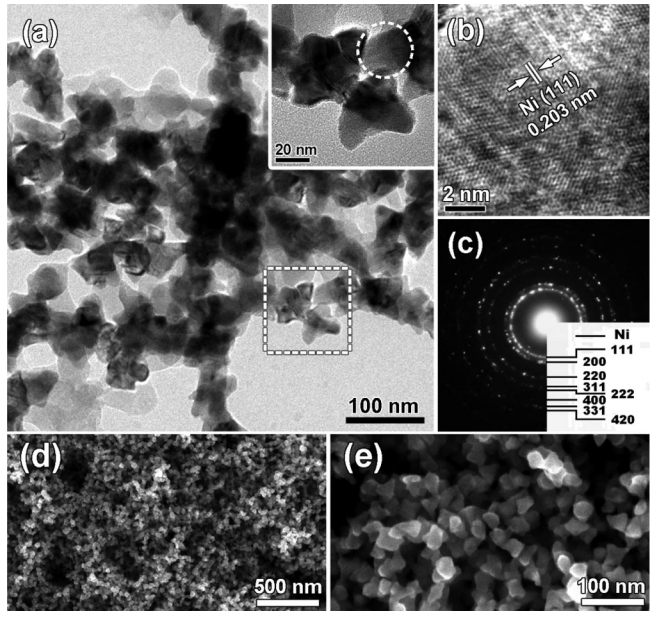

Figure 6. TEM and SEM images of the as-grown starfish-like Ni crystal at 200 °C.

Magnetization of the sample was investigated in a powder collection of 0.84 mg by a SQUID magnetometer. Magnetic properties were characterized by recording both temperature dependence of magnetization, zero-field-cooling (ZFC) and field-cooling (FC), and magnetic field dependence of magnetization. In the ZFC mode, the sample was cooled from room temperature to 5 K. Then a magnetic field of 90 Oe was applied and the magnetization of the sample was measured during the warming process. In the FC mode, the sample was initially cooled from room temperature to 5 K under an applied magnetic field of 10 kOe, and then a subsequent magnetization measurement was recorded from 5 to 300 K in a constant magnetic field of 90 Oe. As shown in Figure 7, MFC(T) and MZFC(T) curves separate from each other as the temperature is increased to 300 K, indicating the presence of an anisotropy barrier. The behavior of the $M(T)$ curves reveals the main feature of thermal activation effect against the barrier, that is, MZFC(T) increases and MFC(T) decreases as the temperature increases. The peak at about 12 K in the MZFC(T) curve is identified as the freezing temperature, T_f, which reveals the defreezing of the frozen moment in the surface layer of particles. This behavior has been observed with the chains of Ni nanoparticles by using PVP as the surface

modifier.[21] Hysteresis loops were measured at 5 and 300 K, respectively. As can be seen from Figure 7, the magnetic saturation is reached with the external field exceeding 5 kOe. It shows a value of saturation magnetization of about 54.2 emu/g and coercivity about 396 Oe for the loop at 5 K, whereas for the loop at 300 K, the values are of 52.3 emu/g and 238 Oe, respectively. Compared to the bulk Ni (ca. ca. 57 emu/g, 0.7 Oe)[22] and that of Ni nanoparticles reported elsewhere (ca. 39.0 emu/g, 176.3 Oe),[23] the Ni nanoflowers exhibit much enhanced coercivity, which may be attributed to the small size of the acicular branches as well as their orderly 3D arrangement. With the increase in temperature, both the coercivity and remnant magnetization decrease due to the thermal activation effect.[24]

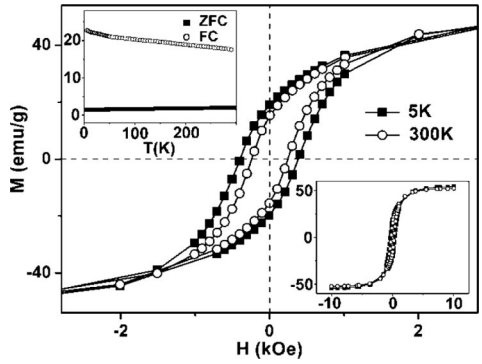

Figure 7. $M(H)$ data measured at 5 and 300 K. The left-top inset shows ZFC and FC magnetization, $M(T)$, with an applied field of 90 Oe. The right shows hysteresis loop in the whole region.

Conclusions

In summary, well-defined flower-like and starfish-like nickel nanocrystals, as well as $[Ni(N_2H_4)_2]Cl_2$ nanorods, were synthesized in the absence of any external field or templates, either hard or soft. It was demonstrated that the solution-based branching growth process is facile and mild, which was suitable to be carried out on a large scale with a low cost. The flower-like nickel nanomaterial also shows enhanced coercivity resulting from the special hierarchical structure. This promises a wide range of applications such as magnetic materials in various fields of modern technology.

Experimental Section

General: All chemicals used in this experiment were of analytical grade and used without further purification. In a typical experiment, ethylene glycol (EG, 40 mL) was first put into a three-necked flask and heated up to 60 °C. Hydrated hydrazine (50%, 10 mL) was then added. After about 5 min, $NiCl_2{\cdot}6H_2O$ (20 mL) dissolved in EG (1×10^{-3} M) was added into the solution stirred by N_2 gas at a flow rate of 20 mL/min. After reaction for 1 h, black products were obtained, filtered, and rinsed with ethanol and deionized water (5–6×). The final products are then preserved in ethanol for further investigation.

The structures and compositions of the as-prepared products were characterized by X-ray powder diffraction (XRD) by using an X′Pert Pro MPD system with Cu-K_α radiation (λ = 1.5416 Å). The XRD specimens were prepared by flattening the powder on the small slides. The morphologies of the synthesized samples were studied by a field-emission gun (FEG) scanning electron microscope (Hitachi S-4800, 10 kV) with the samples obtained from the thick suspension dropping on the silicon slice. Transmission electron microscopy (TEM) and high-resolution TEM (HRTEM) investigations were carried out by a JEOL JEM-2100F microscope. The as-grown samples were dispersed in ethanol and dropped onto a carbon film supported on a copper grid for drying in air. In addition, the magnetic properties of the as prepared nickel nanocrystals were measured by using a superconducting quantum interference device (SQUID) magnetometer (Quantum Design).

Acknowledgments

This work was supported by the National Natural Science Foundation of China (No. 50671003 and 50902007), Beijing Natural Science Foundation (No. 1102025), Research Fund for the Doctoral Program of Higher Education of China (20091102110038), and the Program for New Century Excellent Talents in University (NCET-06-0175).

[1] Y. Huang, X. F. Duan, Q. Q. Wei, C. M. Lieber, *Science* **2001**, *291*, 630–633.
[2] Z. W. Pan, Z. R. Dai, Z. L. Wang, *Science* **2001**, *291*, 1947–1949.
[3] C. J. Murphy, N. R. Jana, *Adv. Mater.* **2002**, *14*, 80–82.
[4] B. I. Kharisov, *Recent Pat. Nanotechnol.* **2008**, *2*, 190–200.
[5] M. Paladugu, J. Zou, Y. N. Guo, X. Zhang, H. J. Joyce, Q. Gao, H. H. Tan, C. Jagadish, Y. Kim, *Angew. Chem. Int. Ed.* **2009**, *48*, 780–783.
[6] X. M. Ni, Q. B. Zhao, J. Cheng, H. G. Zheng, B. B. Li, D. G. Zhang, *Chem. Lett.* **2005**, *34*, 1408–1409.
[7] J. G. Park, W. S. Nam, S. H. Seo, Y. G. Kim, Y. H. Oh, G. S. Lee, U. G. Paik, *Nano Lett.* **2009**, *9*, 1713–1719.
[8] M. Mannini, F. Pineider, P. Sainctavit, C. Danieli, E. Otero, C. Sciancalepore, A. M. Talarico, M. A. Arrio, A. Cornia, D. Gatteschi, R. Sessoli, *Nat. Mater.* **2009**, *8*, 194–197.
[9] F. Y. Cheng, J. Chen, X. L. Gou, *Adv. Mater.* **2006**, *18*, 2561–2564.
[10] R. Y. Zhang, L. Amlani, J. Baker, J. Tresek, R. K. Tsui, *Nano Lett.* **2003**, *3*, 731–735.
[11] I. Sisman, C. Tutunoglu, A. O. Aydin, *Cent. Eur. J. Chem.* **2008**, *6*, 253–257.
[12] S. Ida, D. Shiga, M. Koinuma, Y. Matsumoto, *J. Am. Chem. Soc.* **2008**, *130*, 14038–14039.
[13] D. Navas, M. Hernandez-Velez, M. Vazquez, W. Lee, K. Nielsch, *Appl. Phys. Lett.* **2007**, *90*, 192501.
[14] C. L. Jiang, G. F. Zou, W. Q. Zhang, W. C. Yu, Y. T. Qian, *Mater. Lett.* **2006**, *60*, 2319–2321.
[15] C. S. Tian, D. Qian, D. Wu, R. H. He, Y. Z. Wu, W. X. Tang, L. F. Yin, Y. S. Shi, G. S. Dong, X. F. Jin, X. M. Jiang, F. Q. Liu, H. J. Qian, K. Sun, L. M. Wang, G. Rossi, Z. Q. Qiu, J. Shi, *Phys. Rev. Lett.* **2005**, *94*, 137210.
[16] M. Grzelczak, J. Perez-Juste, B. Rodriguez-Gonzalez, M. Spasova, I. Barsukov, M. Farle, L. M. Liz-Marzan, *Chem. Mater.* **2008**, *20*, 5399–5405.
[17] E. J. Menke, M. A. Thompson, C. Xiang, L. C. Yang, R. M. Penner, *Nat. Mater.* **2006**, *5*, 914–919.
[18] M. Knez, A. M. Bittner, F. Boes, C. Wege, H. Jeske, E. Maiss, K. Kern, *Nano Lett.* **2003**, *3*, 1079–1082.

[19] Y. D. Li, C. W. Li, H. R. Wang, L. Q. Li, Y. T. Qian, *Mater. Chem. Phys.* **1999**, *59*, 88–90.
[20] H. L. Hu, K. Sugawara, *Mater. Lett.* **2008**, *62*, 4339–4342.
[21] N. Wang, X. Cao, D. S. Kong, W. M. Chen, L. Guo, C. P. Chen, *J. Phys. Chem. C* **2008**, *112*, 6613–6619.
[22] J.-H. Hwang, V. P. Dravid, M. H. Teng, J. J. Host, B. R. Elliott, D. L. Johnson, T. O. Mason, *J. Mater. Res.* **1997**, *12*, 1076–1082.
[23] X. M. Ni, Y. F. Zhang, J. M. Song, H. G. Zheng, *J. Cryst. Growth* **2007**, *299*, 365–368.
[24] L. He, C. P. Chen, *Phys. Rev. B* **2007**, *75*, 184424.

Received: January 22, 2010
Published Online: April 9, 2010

